Effect of external drive on strongly coupled Yukawa systems: A nonequilibrium molecular dynamics study

Ashwin J. and R. Ganesh*
Institute for Plasma Research, Bhat, Gandhinagar 382428, India
(Received 21 July 2009; published 30 November 2009)

Using nonequilibrium molecular dynamics (MD) simulations behavior of three-dimensional (3D) Yukawa system has been studied in the presence of a small amplitude drive along one direction (say $\hat{z}$). This drive has the general form $V=V_0\cos(k_L z)\Theta(t-t_0)$, where $\Theta(t-t_0)$ is a Heaviside step function in time at $t=t_0$ and $k_L=2\pi/L$, L being the size of the system; V_0 is considered small compared to average interparticle potential energy. In particular, a 3D equilibrated Yukawa crystal (bcc) near solid-liquid transition is subjected to an external drive at times $t\geq t_0$ at the largest possible scale. For a given k_L it is observed that there exists a critical amplitude (V_0^c) of the external drive below which the crystalline order is preserved and above which $(V_0\geq V_0^c)$ the transition from bcc to strongly coupled Yukawa liquid is observed. This critical amplitude (V_0^c) is sensitive to the location of the Yukawa solid in the (κ,Γ) phase space. Various signatures of melting, transients, and steady state in the presence of this drive are elucidated using extensive MD diagnostics such as loss of long-range crystalline order, change in diffusion from subnormal to normal, and the fall of transversal shear peak in the Fourier transform of the velocity autocorrelation function. The mechanism of heating in the transient state is attributed to the local heating of the system where the forces are maximum. It is shown that these local hot regions dissipate heat into surrounding regions ultimately leading to a uniform temperature throughout the system. Ion streaming due to external field has been neglected.

DOI: 10.1103/PhysRevE.80.056408 PACS number(s): 52.65.Yy, 05.10.−a, 52.27.Lw

I. INTRODUCTION

Yukawa systems provide a testing ground for a large number of fundamental concepts in statistical physics. The formation of dust crystals may be a typical example of interesting behaviors of Yukawa systems [1–5]. In typical laboratory experiments dusty plasma contains electrons, ions, charged microparticles, and a neutral gas background. Experimentally the charged microparticles or dust particles can be individually visualized. They interact electrostatically and the background environment of ions and electrons provide the shielding to their charges. Dusty plasma can be modeled as a Yukawa system which is a collection of particles interacting through Yukawa (i.e., screened Coulomb) pair potential given as

$$\phi(r)=\frac{Q^2}{4\pi\epsilon_0}\frac{\exp(-r/\lambda_D)}{r}, \tag{1}$$

where Q is charge on each dust particle, r is the radial distance between two dust particles, and ϵ_0 is the permittivity of free space. The Debye radius (λ_D), the Wigner-Seitz radius (a), and the dust plasma frequency (ω_p) are given as

$$\lambda_D=\left(\frac{q_i^2\bar{n}_i}{\epsilon_0 k_B T_i}+\frac{e^2\bar{n}_e}{\epsilon_0 k_B T_e}\right)^{-1/2}, \tag{2}$$

$$a=\left(\frac{3}{4\pi n}\right)^{1/3}, \tag{3}$$

$$\omega_p^2=\frac{Q^2 n}{\epsilon_0 m}, \tag{4}$$

where q_i, $\bar{n}_i$, and T_i are the charge, average density, and temperature of the plasma ions, and $-e$, $\bar{n}_e$, and T_e the corresponding quantities for plasma electrons, n is the dust particle number density, and m is the dust particle mass. The thermodynamics of the Yukawa systems is completely described by the following parameters [6]:

$$\kappa=\frac{a}{\lambda_D} \quad \text{and} \quad \Gamma=\frac{Q^2}{4\pi\epsilon_0 a k_B T}. \tag{5}$$

Statistical and thermodynamic properties such as phase transitions [6], transport phenomena [7,8], and dispersion [9] are some of the most fundamental properties characterizing dusty plasma systems. In the past, extensive fluid theoretical analysis have been done for strongly coupled dusty plasmas [10,11]. Equilibrium molecular dynamics studies have tremendously contributed to the understanding of Yukawa systems. Nonequilibrium molecular dynamics (MD) (NEMD) provides a powerful tool to study nonequilibrium features which are difficult to handle analytically. For a given (Γ,κ) pair, it is now well known that a three-dimensional (3D) Yukawa system has a phase diagram composed of face-centered-cubic (fcc), body-centered-cubic (bcc) phases and liquid phases [6]. In typical laboratory experiments dusty plasma exist under external force fields such as gravity and electric fields [12,13]. Under external forces which are confining in nature, it is natural to expect that these dusty plasma will form different structures than the regular fcc and bcc structures. Formation of layers in a dusty plasma in presence of an external confining potential was studied by Totsuji [14,15]. This confining potential had a magnitude much

*ganesh@ipr.res.in

larger than the average interparticle potential energy and the simulations were done in equilibrium conditions. Melting of dusty plasma crystals under spatially random and time varying external fields have also been studied by Hoffman using Fokker-Planck dynamics[16]. In contrast to the above mentioned works, in this paper we study the effect of a small external drive of the form $V=V_0\cos(k_L z)\Theta(t-t_0)$, where $\Theta(t-t_0)$ is the Heaviside step function in time, and $k_L=2\pi/L$, L being the size of the system and V_0 small compared to average interparticle potential energy. The choice of such an external drive is made because any spatial small amplitude perturbation can be represented as an infinite sum of modes (Fourier synthesis) in the system. For simplicity and without loss of generality we have taken the simplest case, taking $k=k_L$ only. The effect of such an external electric drive on a strongly coupled Yukawa system near a solid-liquid phase boundary under both equilibrium and nonequilibrium conditions is addressed. It is important to note that in the presence of an ac external electrical field, ion streaming is known to become significant [17,18]. This ion streaming converts the symmetric Yukawa potential into an asymmetric one including higher-order poles. However in the presence of weak external dc field one may regard the present work as a zeroth-order study, where the ion streaming effects have been neglected. Therefore the Yukawa potential appearing henceforth in this paper is the conventional symmetric potential.

We start from a strongly coupled Yukawa solid (bcc) at thermal equilibrium near solid-liquid phase boundary ($\Gamma=210$, $\kappa=1$) and subject it to an external drive small compared to the average interparticle potential energy. The Yukawa system then goes through a transient phase which involves heating, subsequent loss of long-range crystalline order and melting. We obtain the signatures of melting transition by measuring the statistical properties of the Yukawa system after the transients have died down. An interesting finding of our work is that there exists a critical amplitude of external drive (V_0^c) below which there is no transition into the liquid state. This critical amplitude (V_0^c) is sensitive to the location of the Yukawa solid in the phase space (κ,Γ). At a given κ, the value of V_0^c increases with Γ. A melting mechanism is proposed based upon local heating of the system where the forces are maximum. It is shown that these local hot regions dissipate heat into surrounding regions ultimately leading to a uniform temperature throughout the system.

The organization of this paper is as follows: Sec. II of the paper deals with the molecular dynamics code and the numerical method used, Sec. III presents the molecular dynamics protocol, Sec. IV presents the results, and Sec. V discusses the melting mechanism. Finally we draw the conclusions in Sec. VI.

II. MPMD CODE AND NUMERICAL METHODS

Multipotential molecular dynamics (MPMD) is a parallel molecular dynamics code developed by the authors at the Institute For Plasma Research, Bhat, Gandhinagar-India for simulating Yukawa and Coulomb systems. The code has been exhaustively benchmarked against known results. This code can handle interatomic potentials of Yukawa systems, Lennard-Jones, and Tersoff-Brenner. Ewald sums [19,20] are employed to handle long-ranged forces in the Yukawa system in the presence of periodic boundaries. MPMD can simulate various thermodynamic ensembles such as *NVT*, *NVE*, *NPT* by employing a Gaussian thermostat [21,22] and a Andersen barostat [23]. The reduced units used in MPMD are listed in Table I. Physical quantities appearing henceforth in this paper are in reduced units. We now move on to the following subsections to discuss Ewald sums, thermostats, and the external drive.

TABLE I. Reduced units used in MPMD code.

Reduced quantity	Reduced units
Distance (r)	r/a
Time (t)	$t\omega_p/\sqrt{3}$
Density (ρ)	ρa^3
Temperature (T)	$k_B T(4\pi\epsilon_0 a/Q^2)$
Energy (E)	$E(4\pi\epsilon_0 a/Q^2)$
Force (F)	$F(4\pi\epsilon_0 a^2/Q^2)$
Self-diffusion coefficient (D)	$D\sqrt{3}/(\omega_p a^2)$
Mean-square displacement ($\langle\Delta r^2\rangle$)	$\langle\Delta r^2\rangle/a^2$

A. Ewald sums

We follow Refs. [19,20] to develop the numerical scheme of our MD simulation. Consider a system of N_a atoms, each of which now carries a charge. A periodic array of replicated systems is created in the spirit of the periodic boundary conditions to mimic an infinitely large system; but now, because of the long-range nature of the interactions, the energy of the replicated system includes contributions from all replicas since no truncation is imposed. The interaction energy is now given as

$$\phi(\boldsymbol{r}) = \phi(|\boldsymbol{r}|) + \sum_{\boldsymbol{n}\neq 0} \phi(|\boldsymbol{r}+\boldsymbol{n}L|), \tag{6}$$

with $\phi(r)$ being the Yukawa potential in Eq. (1). L is the size of the simulation box and $\boldsymbol{n}=(n_x,n_y,n_z)$. The contribution from replicated systems becomes important especially if the Debye screening length λ_D becomes comparable to or greater than size of the simulation box L. The above-mentioned potential represents the interaction energy of particle i with particle j (at separation $\boldsymbol{r}=\boldsymbol{r}_j-\boldsymbol{r}_i$) and with all the periodic images of the particles. The infinite sum in Eq. (6) represents the contribution from all the periodic images. In our MD simulations we calculate the total Ewald-Yukawa potential energy of the system by rewriting it as

$$\phi = \phi_r + \phi_k - \phi_{Self}. \tag{7}$$

Here $\boldsymbol{k}=(n_x,n_y,n_z)\frac{2\pi}{L}$. The short-range contribution to Eq. (7) is given as

$$\phi_r = \frac{1}{4}\sum_{ij}{}' \sum_{\boldsymbol{n}} \mathrm{erfc}\left(\alpha|\boldsymbol{r}_{ij}+\boldsymbol{n}L| + \frac{\kappa}{2\alpha}\right)\exp(\kappa|\boldsymbol{r}_{ij}+\boldsymbol{n}L|) + \mathrm{erfc}\left(\alpha|\boldsymbol{r}_{ij}+\boldsymbol{n}L| - \frac{\kappa}{2\alpha}\right)\exp(-\kappa|\boldsymbol{r}_{ij}+\boldsymbol{n}L|), \quad (8)$$

the long-ranged contribution as

$$\phi_k = \frac{2\pi}{V}\sum_{\boldsymbol{k}\neq 0} \frac{\exp\left(-\frac{\boldsymbol{k}^2+\kappa^2}{4\alpha^2}\right)}{\boldsymbol{k}^2+\kappa^2}\left|\sum_i \exp(i\boldsymbol{k}\cdot\boldsymbol{r}_i)\right|^2, \quad (9)$$

and the self interaction is given as

$$\phi_{Self} = \left[\frac{\alpha}{\sqrt{\pi}}\exp\left(\frac{-\kappa^2}{4\alpha^2}\right) - \frac{\kappa}{2}\exp\left(\frac{-\kappa}{2\alpha}\right)\right]. \quad (10)$$

In our simulations the summation over $\boldsymbol{k}$ in Eq. (9) is taken over 297 vectors subject to the constraint $|\boldsymbol{n}| = \sqrt{n_x^2+n_y^2+n_z^2} \leqslant 5$. The value of Gaussian width α is taken as $5.6/L$ [19].

Though we have employed Ewald sums in our MD simulations, for large system size (L) and large screening parameter (κ), Ewald sums are not necessary [24].

B. Thermostats

The choice of thermostats and barostats depends on whether the final states prepared are true ensembles or not. We have used a Gaussian thermostat [21,22] for our work. This thermostat is based on the Gauss's principle of least constraint and results in an isokinetic ensemble. In the limit of large number of degrees of freedom a Gaussian thermostat produces the correct canonical ensemble. The Gaussian thermostat can be build into the Leap-Frog integrator [25]. Because the Gaussian thermostat controls the temperature by the constraint method it gets very close to the desired temperature, and the temperature constraint is only preserved to the accuracy of numerical integration [26]. This can be very useful if one is simulating very large systems. We give here a very simple formulation of the Gaussian thermostat for a system of N_a particles.

$$\frac{1}{2}\sum_{i=1}^{N_a}\dot{\boldsymbol{r}}_i^2 = N_a E_k. \quad (11)$$

Where N_a and E_k are the number of particles and the kinetic energy, respectively. Then the constrained equation of motion is

$$\ddot{\boldsymbol{r}}_i = \boldsymbol{F}_i + \alpha\dot{\boldsymbol{r}}_i \quad (12)$$

and since $\dot{E}_k = 0$ or equivalently $\Sigma_i^{N_a}\dot{\boldsymbol{r}}_i\cdot\ddot{\boldsymbol{r}}_i = 0$, it follows that the value of the Lagrange multiplier α is

$$\alpha = -\frac{\sum_i^{N_a}\dot{\boldsymbol{r}}_i\cdot\boldsymbol{F}_i}{\sum_i^{N_a}\dot{\boldsymbol{r}}_i^2}. \quad (13)$$

The isothermal version of the Leap-Frog integrator is then readily seen to be

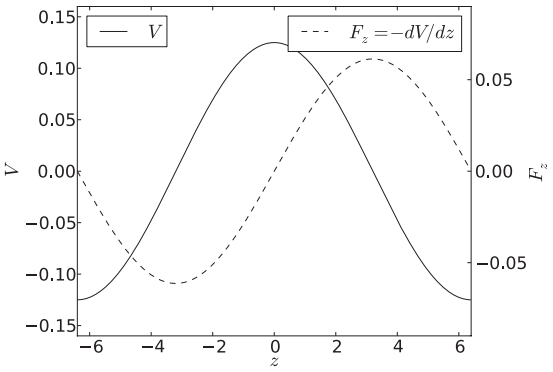

FIG. 1. The external potential V applied along $\hat{z}$ direction and the corresponding force $F_z = -\frac{dV}{dz}$: the cubic simulation box is centered at the origin with the edge length $L = 12.8$. The spatial profile of potential drive is such that the force acting on any particle is always away from the center. Left y axis shows the potential drive and right y axis shows the force in reduced units. Refer to Table I for units.

$$\dot{\boldsymbol{r}}_i(t+\Delta t/2) = (1+\alpha\Delta t)\dot{\boldsymbol{r}}_i(t-\Delta t/2) + \Delta t(1+\alpha\Delta t/2)\boldsymbol{F}_i(t). \quad (14)$$

C. External potential and Hamiltonian

We have applied an external drive along $\hat{z}$ which has the form $V = V_0\cos(k_L z)\Theta(t-t_0)$, where $\Theta(t-t_0)$ is a Heaviside step function in time and $k_L = \frac{2\pi}{L}$ with L being the length of the system. The drive and corresponding force acting at times $t > t_0$ is shown in Fig. 1. Periodic boundaries are employed along $\hat{x},\hat{y},\hat{z}$ directions. The Hamiltonian of the system now becomes,

$$H = \begin{cases} H_0, & t < t_0 \\ H_0 + H_1, & t \geq t_0, \end{cases} \quad (15)$$

where

$$H_0 = \sum_i^{N_a}\frac{v_i^2}{2} + \sum_{i<j}^{N_a}\frac{1}{r_{ij}}\exp(-\kappa r_{ij}) \quad (16)$$

and

$$H_1 = \sum_i^{N_a} V_0\cos(k_L z_i), \quad (17)$$

where z_i is the z coordinate of the particle i. The magnitude of external drive V_0 is small compared to interparticle potential energy. Our system is thus fully described by three parameters; the screening parameter κ, the dimensionless parameter $\Gamma = 1/T$, and strength of the external drive V_0.

III. MOLECULAR DYNAMICS SIMULATIONS

We have performed extensive molecular dynamics simulations with MPMD for three dimensional Yukawa system of dust particles with 432 particles in a cubic box of edge $L = 12.8$. This gives a mean density (ρ) of 0.206. Unless oth-

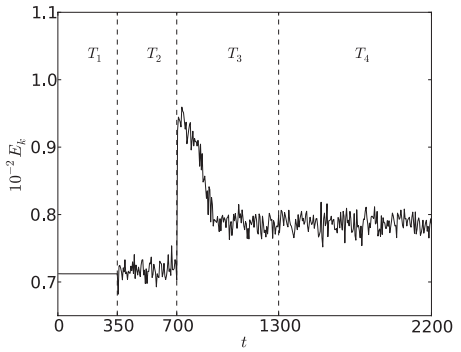

FIG. 2. Steps (i)–(iv) in Sec. III for a given run at $\Gamma=210$, $V_0=0.175$. T_1: canonical run. T_2: microcanonical run. T_3: transient phase. T_4: final equilibrium. Refer to Table I for units.

erwise specified, the screening parameter $\kappa=1$ and inverse temperature $\Gamma=1/T=210$. The Yukawa system for this (κ,Γ) pair is a bcc solid close to the solid-liquid phase boundary. Periodic boundaries were kept along all directions. The time step (Δt) in our MD simulations is 0.001. The simulation is done in the following steps (see Fig. 2 for a typical run at $\Gamma=210$ and $V_0=0.175$):

(i) Canonical run: first we perform canonical ensemble MD for $3.5\times10^5\Delta t$ to take the system to a thermal equilibrium at required $\Gamma=210$ by connecting it to a Gaussian thermostat.

(ii) Microcanonical run: after step (i), we remove the thermostat and do a microcanonical MD for $3.5\times10^5\Delta t$ where the system finds a different thermal equilibrium very close to the Γ set in step (i). At this stage measurements with $V_0=0$ are taken.

(iii) Transient phase: at the end of step (ii) (and the thermostat decoupled), the external drive is turned on and the system goes through transient phase where the temperature of the system changes. Measurements in nonequilibrium conditions is done during this phase.

(iv) Final equilibrium: we continue the simulations after step (iii) until the transients die and the final equilibrium is reached. At this stage equilibrium measurements with $V_0\neq0$ are taken.

We now move on to Sec. IV to discuss the results of our simulations.

IV. RESULTS

In this section we present our results in both the nonequilibrium (transient) and equilibrium conditions. Section IV A discusses the energetics of our simulations, Sec. IV B deals with the measurements on the lattice structure, Sec. IV C deals with the self-diffusion coefficient and mean-square displacement and finally in Sec. IV D we discuss the Fourier transformed velocity autocorrelation function.

A. Energetics

We give the time evolution of energies with the time axis divided into the following three regions:

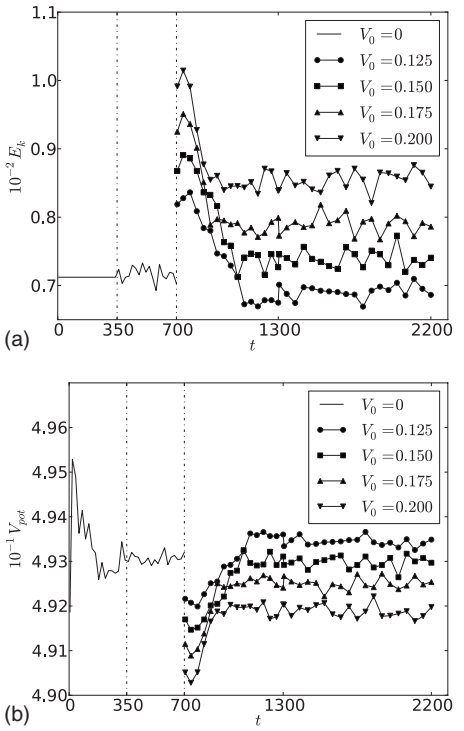

FIG. 3. (a) Kinetic energy per particle (E_k) vs time: the sudden rise in temperature is clearly seen at $t=700$. This rise in T is followed by a fall, which is due to the rearrangement of the Yukawa system in the external drive. (b) Potential energy per particle (V_{pot}) vs time: the time evolution of potential energy is consistent with the kinematics. The Yukawa system slowly reaches its final equilibrium in presence of external drive at time $t\approx1300$. Refer to Table I for units.

(a) $0\leq t<350$: canonical run: thermostat on, external drive off.

(b) $350\leq t<700$: microcanonical Run: thermostat off, external drive off.

(c) $700\leq t<1300$: transient Phase: thermostat off, external drive on.

(d) $1300\leq t<2200$: final equilibrium: thermostat off, external drive on.

As the external drive has the form $V=V_0\cos(k_Lz)$; $k_L=\frac{2\pi}{L}$, the total energy of the Yukawa system should not change when the external drive is turned on provided the particles are arranged symmetrically around $z=0$. However, since we have a thermally equilibrated Yukawa solid, the arrangement of particles is not symmetric around the $z=0$ plane. As can be expected this leads to a small jump in the total energy at the instant the Yukawa solid is subjected to the external drive. In the present work this jump is more than two orders of magnitude smaller than the variations in kinetic and potential energies. Hence our energetics are well resolved. In Figs. 3(a) and 3(b) we show the time evolution of kinetic and potential energies, respectively.

B. Structure

1. Lattice correlation

Long-range order corresponds to the presence of lattice structure and is the quantity underlying x-ray scattering mea-

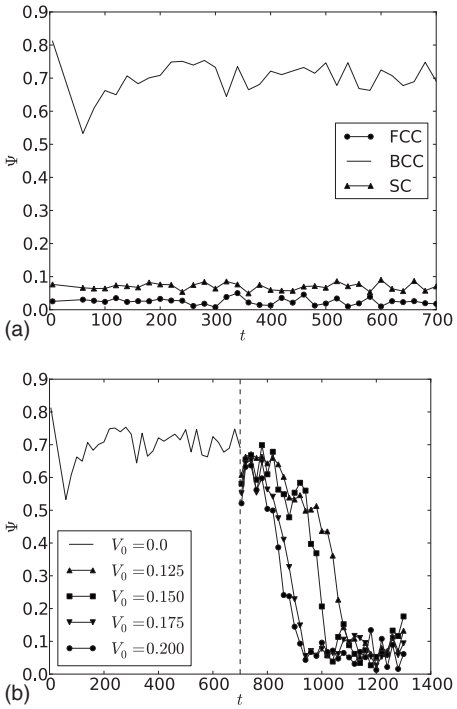

FIG. 4. (a) Lattice correlation (Ψ) without external drive: the long-range lattice order is bcc in the absence of external drive. (b) Lattice correlation (Ψ) with external drive: the drive is switched on at $t=700$. The fall in lattice order is clearly faster with increasing V_0.

surements from crystalline materials. If the local density at a point r can be expressed as a sum over atoms:

$$\rho(\boldsymbol{r}) = \sum_{j=1}^{N_a} \delta(\boldsymbol{r} - \boldsymbol{r}_j), \tag{18}$$

then its Fourier transform is simply the lattice correlation Ψ

$$\Psi = \frac{1}{N_a} \sum_{j=1}^{N_a} \exp(-i\boldsymbol{k} \cdot \boldsymbol{r}_j). \tag{19}$$

In calculations of Ψ done to test the presence of long-range order we take the values of k as $\frac{2\pi}{l_u}(1,-1,1)$, $\frac{2\pi}{l_u}(1,0,1)$, and $\frac{2\pi}{l_u}(1,0,0)$ for face-centered-cubic, body-centered-cubic, and simple cubic lattices, respectively, and l_u is unit cell edge. If the system is almost fully ordered then $\Psi \approx 1$ but in the disordered liquid state $\Psi \approx O(N_a^{-1/2})$. The initial crystalline structure of our system of 432 particles at $\Gamma=210$ and $\kappa=1$ is bcc. as shown in Fig. 4(a). In Fig. 4(b) we show the melting of the system and loss of crystalline order with the application of external drive.

2. Radial distribution function

The fluid state is characterized by absence of any permanent structure. In the case of spatially homogeneous systems only relative separation is meaningful [26], and hence we use the following sum over all pairs for the radial distribution function:

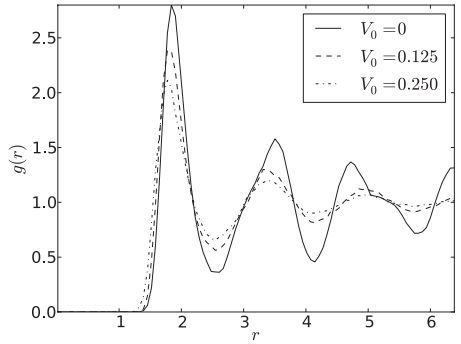

FIG. 5. Radial distribution function $g(r)$: the fall in the peaks of $g(r)$ is clearly seen with varying amplitudes of external drive V_0. The oscillations in $g(r)$ even for larger values of V_0 indicate that the transition is from solid state to a strongly coupled liquid state.

$$g(\boldsymbol{r}) = \frac{2V}{N_a^2} \left\langle \sum_{i<j} \delta(\boldsymbol{r} - \boldsymbol{r}_{ij}) \right\rangle. \tag{20}$$

Since $g(r)$ is a function that gives spherically averaged local organization around any atom, $\rho g(r) d\boldsymbol{r}$ is proportional to the probability of finding an atom in the volume element $d\boldsymbol{r}$ at a distance $\boldsymbol{r}$ from a given atom. Spherically averaged $g(r)$ for various values of external drive V_0 is shown in Fig. 5. For $V_0=0$, $g(r)$ is measured after the system has reached equilibrium, and for $V_0 \neq 0$, $g(r)$ is measured when the system has reached equilibrium in the presence of the external drive. As V_0 increases the peaks in $g(r)$ decrease which shows the loss of long-range positional order as the system goes toward the liquid state. For $V_0=0.125$ the first peak in $g(r)$ falls by about 18%, and at $V_0=0.250$ it falls by 25%. At finite V_0, although the system has lost lattice order [see Fig. 4(b)], it is still a correlated liquid as seen from the oscillations in $g(r)$. In the following subsection we discuss the diffusion properties of Yukawa solid in the presence of external drive.

C. Self-diffusion coefficient and mean-square displacement

The self-diffusion coefficient in the long time limit is given by Einstein relation

$$D = \lim_{t\to\infty} \frac{1}{6N_a t} \left\langle \sum_{j=1}^{N_a} [\boldsymbol{r}_j(t) - \boldsymbol{r}_j(0)]^2 \right\rangle. \tag{21}$$

We define mean-square displacement as

$$\langle \Delta r^2 \rangle = \frac{1}{N_a} \left\langle \sum_{j=1}^{N_a} [r_j(t) - r_j(0)]^2 \right\rangle. \tag{22}$$

Then from Eqs. (21) and (22), we get

$$\langle \Delta r^2 \rangle = 6Dt. \tag{23}$$

The angular brackets $\langle \cdots \rangle$ stand for ensemble average over 400 ensembles at equilibrium. All the measurements were done after step (ii) (for $V_0=0$) and step (iv) (for $V_0 \neq 0$) as mentioned in Sec. III. For liquids and gases at long times, $\langle \Delta r^2 \rangle$ goes as t and hence D asymptotes to a constant value. This constant value is called the diffusion coefficient

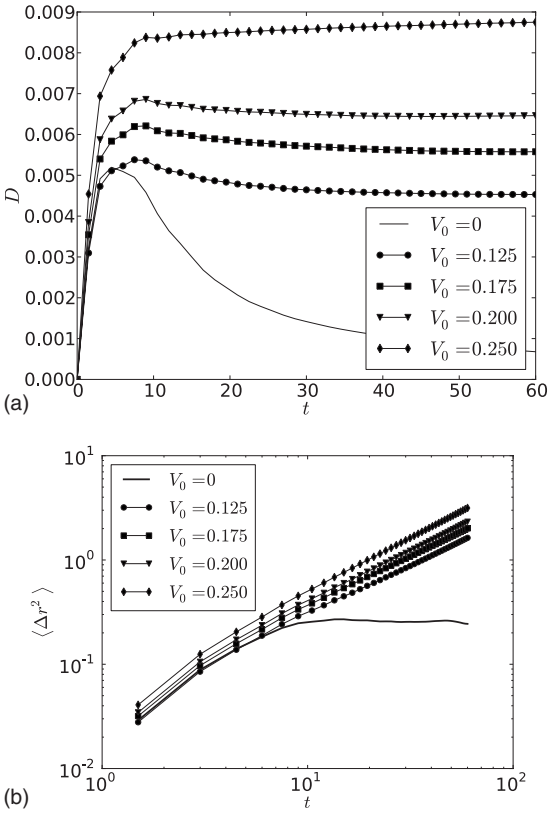

FIG. 6. (a) Diffusion: for V_0 there is no diffusion, but higher values of V_0 show that the diffusion asymptotes to larger values. (b) Mean-square displacement $\langle \Delta r^2 \rangle$ on a log-log scale: except for $V_0=0$ where the displacement is limited, higher values show $\langle \Delta r^2 \rangle$ increasing linearly with time. Refer Table I for units.

of the system. In Figs. 6(a) and 6(b) we show the plots for D and $\langle \Delta r^2 \rangle$, respectively, for our system at equilibrium. It is clear from these figures that for smaller values of V_0, D drops close to zero (there is no diffusion). This is characteristic of solid state. At higher values of V_0, D asymptotes to higher values. This asymptotic nature of D is a typical characteristic of liquid state. In the following section we discuss the velocity autocorrelation and its Fourier transforms.

D. Fourier transformed velocity autocorrelation function

The normalized velocity autocorrelation function is constructed as

$$Z(t) = \frac{\left\langle \sum_{j=1}^{N_a} \boldsymbol{v}_j(t) \cdot \boldsymbol{v}_j(0) \right\rangle}{\left\langle \sum_{j=1}^{N_a} \boldsymbol{v}_j(0) \cdot \boldsymbol{v}_j(0) \right\rangle}, \tag{24}$$

Its Fourier transform $Z(\omega)$ is given as

$$Z(\omega) = \frac{1}{2\pi} \int_{-\infty}^{\infty} Z(t) \exp(i\omega t) dt. \tag{25}$$

The integral in Eq. (25) is approximated as a discrete sum and calculated via fast Fourier transform of $Z(t)$

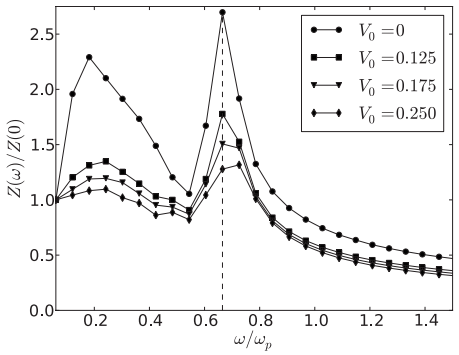

FIG. 7. Fourier transformed velocity autocorrelation: as V_0 increases the longitudinal peak at $\omega \approx 0.67\omega_p$ begins to fall. There is also a clear fall in the low frequency transversal shear peak as V_0 increases (see text for explanation).

$$Z(\omega) \approx \sum_{n=0}^{N-1} Z(t_n) \exp(i\omega t_n) \Delta t. \tag{26}$$

The power spectrum of $Z(\omega)$ for various values of V_0 are plotted in Fig. 7. In the strong coupling regimes ($\Gamma=210$), the power spectrum of $Z(\omega)$ shows a collective peak near plasmon frequency at $\omega \approx 0.67\omega_p$ as shown in previous works [27]. There is another prominent peak near a low nonzero frequency. To explain this peak Hansen, McDonald and Pollock attempted to give a unified description of the velocity autocorrelation function in the liquid regime using the memory function formalism [28]. A somewhat more general approach in sort of a mode coupling model was investigated by Gold and Mazenko [29]. It was shown by Schmidt for coulomb liquids [30] that this low-frequency peak at strong coupling is associated with the occurrence of transversal acoustic excitations (or shear modes) in the system. We notice two important trends here: first, the collective peak near the plasmon frequency ω_p starts to fall and second, the broad peak at low frequency which corresponds to shear modes starts to disappear. Both these observations confirm the approach to the liquid state as the external drive V_0 increases. In the following section we discuss the melting mechanism of Yukawa solid in the presence of an external drive.

V. MECHANISM OF MELTING

The applied external drive results in a force along $\hat{z}$ with a sinusoidally varying magnitude. It is interesting to note that work done due to this directed force is being converted into random kinetic energy of particles due to collisions with nearest neighbors. In this section, we attempt to give a qualitative explanation for the melting mechanism. At the instant when the external drive is turned on local hot zones are created where the magnitude of forces is maximum [see Fig. 8(a)]. These hot zones give heat to the neighboring region and the system heats up. At the beginning of the transient phase the two humps in the temperature are clearly seen. These humps vanish toward the end of the transient phase. We define the temperature profile along $\hat{z}$ as follows:

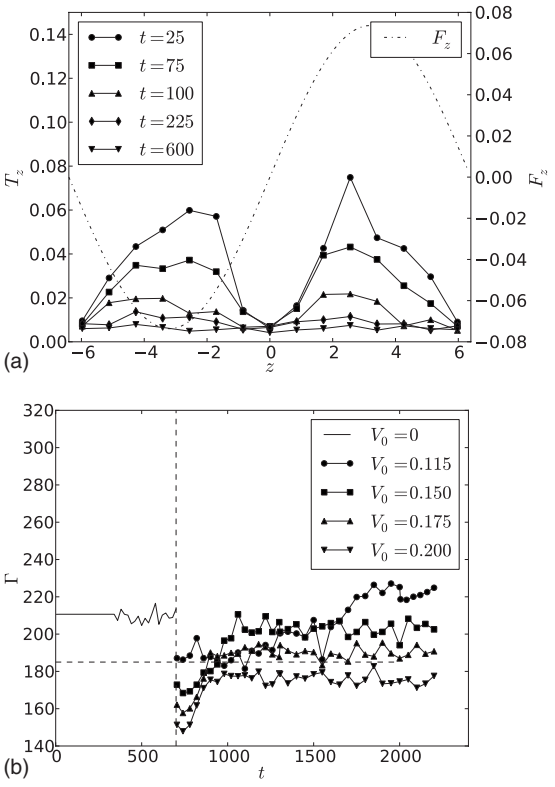

FIG. 8. (a) Snapshots of temperature along $\hat{z}(T_z)$ taken at different times. The z component of force F_z (taken on right y axis) is plotted on top. The figure explains initial local heating in regions where magnitude of F_z is maximum. The simulation box is centered at origin. (b) The plot of Γ as a function of time for various values of V_0. Horizontal dotted line shows the $\Gamma=185$ solid-liquid phase boundary line for $\kappa=1$. See [6].

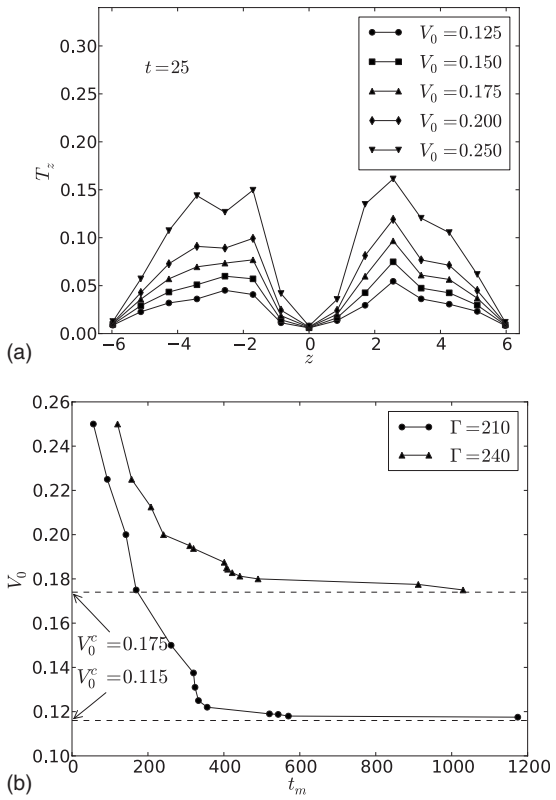

FIG. 9. (a) The profile of temperature along $\hat{z}(T_z)$ very early in the run ($t=25$) for various values of V_0. (b) The melting time (t_m) versus V_0 for two values of initial Γ. t_m is the time during which the lattice correlation Ψ fall by an efold ($\approx 37\%$). From this graph we compute V_0^c as the value at which the Yukawa solid takes infinite time to melt into a liquid. Dashed lines cut the x axis at V_0^c. At higher Γ, value of V_0^c is higher.

$$T_z = \left\langle \frac{1}{N_z} \sum_i^{N_z} \frac{1}{2} v_i^2 \right\rangle, \tag{27}$$

where N_z is the number of particles in one of the slabs along $\hat{z}$ and $\langle\ \rangle$ denote the time average. In Fig. 8(a) we show the temperature profile (T_z) along $\hat{z}$ for the case $V_0=0.150$.

In Fig. 8(b) we show the plots of inverse temperature (Γ) as a function of time for various values of V_0. For each value of V_0, the initial Γ falls before reaching an equilibrium value. For the case $V_0=0.115$, the fall in Γ is just as much so that the Yukawa system comes close to the solid-liquid phase boundary which is at $\Gamma=185$ for $\kappa=1$ (horizontal dotted line [6]). It is interesting to note that at late times the value of Γ for $V_0=0.115$ case is marginally higher than the initial value. From this figure we qualitatively explain that the critical amplitude of melting V_0^c should be close to 0.115.

It was shown in the Fig. 4(b) that the fall of lattice correlation (Ψ) is rapid as we increase the value of V_0. We define the melting time t_m as the time in which Ψ falls by an efold ($\approx 37\%$). In Fig. 9(a), for a given initial temperature ($\Gamma=210$) we show the temperature profile along $\hat{z}$ very early in the run ($t=25$) for different values of V_0. The increased local heating is clearly seen with increasing values of V_0. This qualitatively explains the decrease in melting times with increasing V_0. In Fig. 9(b) we show V_0 versus melting times for different values of initial temperatures ($\Gamma=200$ and $\Gamma=240$). At higher Γ, the correlations in the Yukawa system get stronger and hence it may be expected that the critical amplitude (V_0^c) is larger. This feature is clearly seen in Fig. 9(b).

VI. CONCLUDING REMARKS

We have performed for the first time extensive equilibrium and nonequilibrium molecular dynamics simulations on 3D Yukawa systems with periodic boundary conditions along $\hat{x}$, $\hat{y}$, and $\hat{z}$ under an external drive given by $V=V_0\cos(k_L z)\Theta(t-t_0)$, where $\Theta(t-t_0)$ is a Heaviside step function in time and $k_L=2\pi/L$, L being the size of the system. The long-range nature of the force and the periodic boundaries were properly handled by including Ewald sums. The initial state of the system of 432 particles is a regular BCC state. We then apply a small external drive and observe the melting of the system. After the initial transients die down we measure statistical properties such as the self-diffusion coefficient, mean-square displacement, and Fourier transformed velocity autocorrelation functions. The solid to liquid melting is discussed on the basis of these statistical

properties and a mechanism for melting is proposed based on local heating in the system in regions where the magnitude of forces are maximum. We also qualitatively explain the decrease in melting times with increasing the magnitude of external drive V_0. For a given (Γ,κ) pair we have found a critical amplitude of external drive V_0^c below which there is no transition. This critical amplitude (V_0^c) depend on the location of the Yukawa system in the (κ,Γ) phase space. For larger Γ, the value of V_0^c is larger. There are several open questions such as the effect of the external drive at multiple $k_L's$, scaling of V_0^c with the screening parameter κ, and characterization of the nature of transition of Yukawa solid to a strongly correlated liquid. As a comparison, more rigorous potential models, such as the asymmetric Yukawa potential [17,18] can be employed to study similar phenomena.

ACKNOWLEDGMENTS

The authors would like to thank P. K. Kaw and M. Warrier for a critical reading of the paper. Special thanks to M. Warrier for discussions on MD techniques. The MD code for this work was developed by the authors and was run on Institute For Plasma Research's cluster. The authors would like to give special thanks to Deepak Sangwan, S. K. Singh, and Rameswar Singh for providing their workstations for running our MD code.

[1] H. Thomas, G. E. Morfill, V. Demmel, J. Goree, B. Feuerbacher, and D. Möhlmann, Phys. Rev. Lett. **73**, 652 (1994).
[2] J. H. Chu and L. I, Phys. Rev. Lett. **72**, 4009 (1994).
[3] Y. Hayashi and K. Tachibana, Jpn. J. Appl. Phys. **33**, L804 (1994).
[4] A. Melzer, T. Trottenberg, and A. Piel, Phys. Lett. A **191**, 301 (1994).
[5] H. Ikezi, Phys. Fluids **29**, 1764 (1986).
[6] S. Hamaguchi, R. T. Farouki, and D. H. E. Dubin, Phys. Rev. E **56**, 4671 (1997).
[7] T. Saigo and S. Hamaguchi, Phys. Plasmas **9**, 1210 (2002).
[8] Z. Donkó and P. Hartmann, Phys. Rev. E **69**, 016405 (2004).
[9] H. Ohta and S. Hamaguchi, Phys. Rev. Lett. **84**, 6026 (2000).
[10] M. A. Berkovsky, Phys. Lett. A **166**, 365 (1992).
[11] P. K. Kaw and A. Sen, Phys. Plasmas **5**, 3552 (1998).
[12] B. Liu and J. Goree, Phys. Rev. Lett. **100**, 055003 (2008).
[13] P. Bandyopadhyay, G. Prasad, A. Sen, and P. K. Kaw, Phys. Rev. Lett. **101**, 065006 (2008).
[14] H. Totsuji, Phys. Plasmas **8**, 1856 (2001).
[15] H. Totsuji, T. Kishimoto, and C. Totsuji, Phys. Rev. Lett. **78**, 3113 (1997).
[16] G. P. Hoffmann and H. Lowen, J. Phys.: Condens. Matter **12**, 7359 (2000).
[17] R. Kompaneets, G. E. Morfill, and A. V. Ivlev, Phys. Plasmas **16**, 043705 (2009).
[18] A. V. Ivlev *et al.*, Phys. Rev. Lett. **100**, 095003 (2008).
[19] G. Salin and J. Cailol, J. Chem. Phys. **113**, 10459 (2000).
[20] M. Mazars, J. Chem. Phys. **126**, 056101 (2007).
[21] D. J. Evans, W. G. Hoover, B. H. Failor, B. Moran, and A. J. C. Ladd, Phys. Rev. A **28**, 1016 (1983).
[22] D. J. Evans, J. Chem. Phys. **78**, 3297 (1983).
[23] H. C. Andersen, J. Chem. Phys. **72**, 2384 (1980).
[24] B. Liu and J. Goree, Phys. Rev. Lett. **94**, 185002 (2005).
[25] D. Brown and J. Clarke, Mol. Phys. **51**, 1243 (1984).
[26] D. C. Rapaport, *The Art of Molecular Dynamics Simulation* (Cambridge University Press, New York, 1995).
[27] Z. Donkó, G. J. Kalman, and P. Hartmann, J. Phys.: Condens. Matter **20**, 413101 (2008).
[28] J. P. Hansen, I. R. McDonald, and E. L. Pollock, Phys. Rev. A **11**, 1025 (1975).
[29] H. Gould and G. F. Mazenko, Phys. Rev. Lett. **35**, 1455 (1975).
[30] P. Schmidt, G. Zwicknagel, P. G. Reinhard, and C. Toepffer, Phys. Rev. E **56**, 7310 (1997).